Electronic structure of Fe-based amorphous alloys studied using electron-energy-loss spectroscopy

H. J. Wang,[1] X. J. Gu,[2] S. J. Poon,[2] and G. J. Shiflet[1]
[1]*Department of Materials Science and Engineering, University of Virginia, Charlottesville, Virginia 22904, USA*
[2]*Department of Physics, University of Virginia, Charlottesville, Virginia 22904, USA*
(Received 3 January 2007; revised manuscript received 25 April 2007; published 16 January 2008)

The local atomic electronic structures of Fe-Mo-C-B metallic glasses are investigated using electron energy-loss spectroscopy (EELS). The fracture behavior of this Fe-based amorphous alloy system undergoes the transition from being ductile to exhibiting brittleness when alloyed with Cr or Er atoms. In addition, the glass-forming ability is also enhanced. This plastic-to-brittle transition is suggested to correlate with the change of local atomic short-range order or bonding configurations. Therefore, the bonding configuration of Fe-Mo-C-B-Er(Cr) amorphous alloys is investigated by studying the electronic structure of Fe and C atoms using electron energy-loss spectroscopy. It is shown that the normalized EELS white line intensities of Fe-$L_{2,3}$ edges decrease slightly with an increasing amount of Er additions, while no noticeable difference is obtained with Cr additions. As for the C *K* edge, a prominent change of edge shape is observed for both alloy systems, where the first peak corresponding to a $1s \rightarrow 1\pi^*$ transition increases with increasing Er and Cr additions. Accordingly, it is concluded that changes in the local atomic and electronic structure occur around Fe and C atoms when Er and Cr are introduced into the alloys. Furthermore, it is pointed out that the formation of Er-C and Cr-C carbide like local order inferred from the observed C *K* edge spectra can provide a plausible explanation for the plastic-to-brittle transition observed in these Fe-based amorphous alloys. In spite of the complexity of electronic and atomic structure in this multicomponent Fe-based metallic glass system, this study could serve as a starting point for providing a qualitative interpretation between electronic structure and plasticity in the Fe-Mo-C-B amorphous alloy system. Complimentary techniques, such as x-ray diffraction and high-resolution transmission electron microscope are also employed, providing a more complete structural characterization.

DOI: 10.1103/PhysRevB.77.014204 PACS number(s): 61.43.Dq, 79.20.Uv

I. INTRODUCTION

Since the development of Fe-based bulk metallic glasses, there is an increasing interest in these alloys as structural materials because of several attractive physical properties. These properties include high strength and hardness, corrosion and wear resistance, coupled with relatively low materials cost. However, the lack of plasticity has limited the development of Fe-based metallic glasses as structural materials. Recently, an Fe-Mo-C-B bulk metallic glass with the composition of $Fe_{65}Mo_{14}C_{15}B_6$ has been found to exhibit some plasticity (ca. 0.8% in compression).[1] A ductile-to-brittle transition occurs when lanthanide (Ln) elements or Cr are added with the purpose of enhancing the glass formability.[2] Most studies on Fe-based metallic glass systems primarily focus on understanding the excellent soft magnetic properties of the alloys, as well as the methods of enhancing glass formability through empirical alloying strategies and atomic packing processes.[3,4] With rising interest and importance regarding Fe-based metallic glasses, a more broad understanding in the factors determining plastic performance is required.

Generally, the differing behaviors in hardness and softness, or brittleness and ductility in a solid material are related to a difference in resistance to plastic flow.[5] Since all the metallic glasses exhibit a dislocation-free homogeneous amorphous structure, the factor which could possibly determine the level of plastic resistance is considered directly related to chemical bonding. At a most fundamental level, the interatomic forces, i.e., bonding, are determined by local electronic structure. Investigating the changes and differences in bonding configurations among these alloys with various Er or Cr additions that cross the ductile-to-brittle chemical regime is a first step towards constructing the correlation between plasticity and electronic structure.

The base Fe-Mo-C-B bulk metallic glass selected for the present investigation contains two transition metals and two metalloid elements. Carbon is the main metalloid element because of its important role in forming bonds with all transition metals and lanthanides. As a result, a better understanding concerning the electronic structure and bonding configuration associated with carbon atoms should lead to more detailed information about how bonding configuration affects plasticity. In addition, Fe is the dominant element (>50 atomic fraction). The change of electronic structure around Fe through alloying will offer information about bonding configurations and bonding formation. Therefore, a practical first step is to begin an investigation of the Fe electronic structure with various Er or Cr additions. The existence of metal-metal, metal-metalloid, and metalloid-metalloid bonding makes the analysis of the electronic structure within the alloys extremely difficult because of the complexity of bonding configurations. Consequently, the current electronic structure study will be focused only on C, Cr, and Fe atoms.

Electron energy-loss spectroscopy (EELS) is employed to carry out the electronic structure study. This tool provides detailed information on the chemical environment of excited atoms. In transition metals, there may be a large density of unoccupied *d* states above the Fermi level, yielding prominent "white lines" in the near-edge structure of an EELS spectrum. The white lines, which generally contain double sharp peaks at threshold, arise through transitions from the

$2p$ core levels to the narrow unoccupied d states in the transition elements, in which the lowest in energy is the transition from the $2p_{3/2}$ level (L_3 edge) separated from the $2p_{1/2}$ transition (L_2 edge) by spin-orbit splitting. One piece of information that may be obtained from examining white lines is the electron transfer that occurs between outer d states of transition metal atoms upon alloying, or during solid-state phase transformations. Pearson *et al.*[6] have concluded that the integrated intensities of white lines (or the sum of L_2 and L_3 edge intensities), normalized to the trailing background, decrease nearly linearly with increasing atomic number, reflecting the filling of the d states. Therefore, changes in the integrated white line intensity (relative to the trailing background) can be correlated directly to changes in the number of d electron holes, i.e., charge transfer. As for the C K edge, two transitions, which are $1s \rightarrow \sigma^*$ and $1s \rightarrow 1\pi^*$ transitions corresponding to the different symmetries of the s-p-d hybridization bonding states, can be observed in the K edge depending on the bonding configuration that the C atom exhibits. By analyzing the changes associated with $1s \rightarrow \sigma^*$ and $1s \rightarrow 1\pi^*$ edges, bonding configuration around C can be revealed.

The analysis will involve a discussion of the difference in bonding, electronic interactions among elements, and information on the unoccupied d state of Fe among different Fe-based alloys with or without additions of Er or Cr. This study will focus on examining the correlation between electronic structure and plasticity in the Fe-Mo-C-B bulk metallic glass system by varying the contents of Er and Cr additions.

II. EXPERIMENTAL PROCEDURE

$Fe_{65-x}Mo_{14}C_{15}B_6Er_x$ and $Fe_{65-x}Cr_xMo_{14}C_{15}B_6$ ingots were prepared in a titanium-gettered, arc-melting furnace under an Ar environment. Cylindrical samples were produced by suction casting of the molten alloys into a copper mold. Amorphous ribbons were prepared using the single-roller melt-spinning technique. The prepared samples were examined using x-ray diffraction (XRD) and conventional transmission electron microscopy (TEM) at 200 kV. High-resolution TEM imaging was done on a top entry 400 kV TEM. Electron energy-loss spectra (EELS) were acquired using a field-emission analytical TEM equipped with a Gatan Model 678 Imaging Filter (GIF). Low loss and core edge EELS spectra were taken on different areas of the samples using either image mode or diffraction mode at various magnifications. The same background-subtracted window was applied to all spectra corresponding to the same edge. A large illumination area was used during acquisition so radiation damage on the samples could be minimized. Finally, normalized $3d$ white line intensities calculations were obtained from more than ten spectra for increased accuracy. Two series of alloy systems, $Fe_{65-x}Mo_{14}C_{15}B_6Er_x$ with $x=0$, 0.5, 1, and 2, and $Fe_{65-x}Cr_xMo_{14}C_{15}B_6$ with $x=0$, 6, and 15, were used to carry out the investigations. Mo, C, and B contents are fixed for all the alloys so variations induced by them can be minimized, and in this report are neglected.

III. RESULTS AND DISCUSSION

A. TEM and XRD results

Figure 1(a) shows the XRD (Cu $K\alpha$) results for the $Fe_{65-x}Mo_{14}C_{15}B_6Er_x$ amorphous alloys. All XRD patterns exhibit a diffuse hump curve, indicating a complete amorphous structure of the samples. The amorphicity of the samples is further confirmed by TEM diffraction, high-resolution TEM studies, and differential scanning calorimetry (DSC) signatures. A representative TEM diffraction pattern and high-resolution image acquired on an as-spun $Fe_{65}Mo_{14}C_{15}B_6$ amorphous alloy are presented in Fig. 1(b). Concentric diffuse rings in the diffraction pattern and a maze or mottled underfocused image in the high-resolution TEM image correspond to a lack of a long-range ordered structure. Similar amorphous XRD results are obtained for $Fe_{65-x}Cr_xMo_{14}C_{15}B_6$ as well (not shown here). Chemical analysis is verified using the EDXS technique and the results corresponding to $Fe_{65-x}Mo_{14}C_{15}B_6Er_x$ amorphous alloys are given in Fig. 2, which shows the Er peak intensity increases with increasing Er additions.

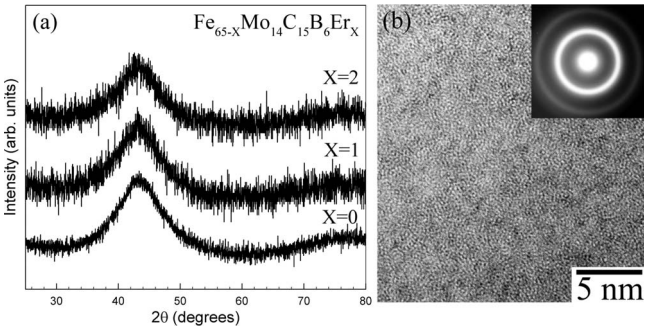

FIG. 1. (a) The XRD results of $Fe_{65-x}Mo_{14}C_{15}B_6Er_x$ amorphous alloys, and (b) the diffraction pattern and HREM image of the as-spun $Fe_{65}Mo_{14}C_{15}B_6$ alloy.

B. C K edge

The background-subtracted and plural scattering removed C K-edge EELS spectra corresponding to as-cast $Fe_{65-x}Mo_{14}C_{15}B_6Er_x$ and $Fe_{65-x}Cr_xMo_{14}C_{15}B_6$ amorphous alloys are shown in Fig. 3. All plots are normalized with respect to the maximum of the $1s \rightarrow \sigma^*$ transition peak and the tailed background. (The C K-edge position is calibrated by

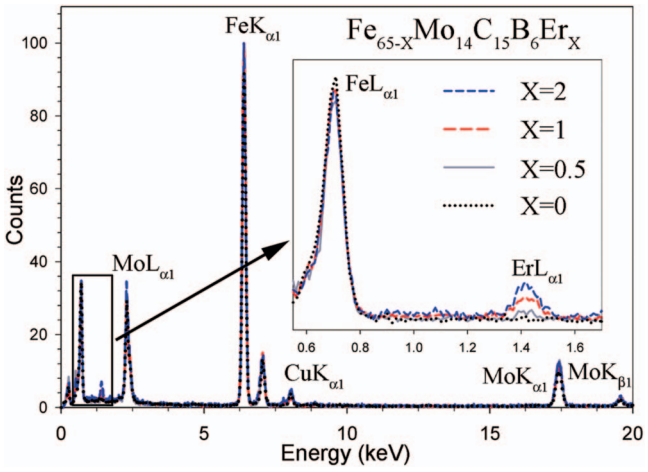

FIG. 2. (Color) The EDXS results of $Fe_{65-x}Mo_{14}C_{15}B_6Er_x$ amorphous alloys.

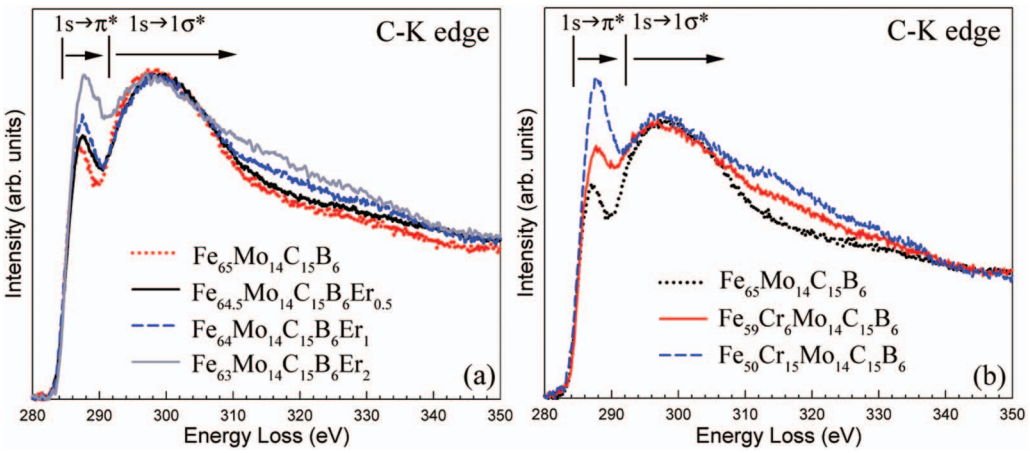

FIG. 3. (Color) C *K*-edge spectra corresponding to (a) $Fe_{65-x}Mo_{14}C_{15}B_6Er_x$ and (b) $Fe_{65-x}Cr_xMo_{14}C_{15}B_6$ amorphous alloys.

utilizing the C *K*-edge spectrum of single crystalline SiC alloy acquired with energy dispersion of 0.1 eV/pixel.) From Fig. 3, all spectra show patterns similar to amorphous carbon, which contains both σ and π bonding configurations.[7] Also, the edge position is found not to vary among the samples. Another common feature observed in the C *K*-edge spectra is that the intensity of the $1s \rightarrow 1\pi^*$ transition peak increases with increasing Er or Cr content. This result indicates that the number of π bonds increase around C atoms when Er or Cr atoms are introduced into the alloys.

For metallic glasses comprised of metals and metalloids, the solute (metalloid) atoms are shown to be surrounded by the metal atoms in forming the so-called solute centered clusters in the amorphous matrix.[8] Therefore, in Fe-Mo-C-B-Er(Cr) amorphous alloys, the formation of π bonds around C atoms can be attributed to the hybridization of C *p*-state electrons with the outer *d*-state electrons of *M* (transition metal) atoms. Without the additions of Er and Cr, the C *K*-edge spectrum of $Fe_{65}Mo_{14}C_{15}B_6$ is observed to resemble the C *K*-edge spectrum reported for amorphous carbon, which can be attributed to the noncrystalline local bonding environment of the carbon atoms. Moreover, the amorphous nature of the spectrum also suggests that the Fe and Mo atoms are distributed homogeneously in the amorphous structure. By introducing the Er and Cr atoms into the base alloy, strong Er-C and Cr-C bonds are preferentially formed because of the relatively large heat of mixing between Er (Cr) and C atoms. In view of the strong Er-C or Cr-C association, there is a tendency for the newly introduced Er or Cr atoms to occupy the atomic sites shared by two or more clusters. The formation of Er-C or Cr-C short-range order in the intercluster regions could contribute to the efficient packing of clusters in the amorphous structure.[9,10] It is plausible that the Cr-C and Er-C short-range order might also resemble the local structure of crystalline carbide. Although further study will be needed to reveal the exact nature of the local structure, it is noted that the C *K* edge spectra that exhibit a strong $1s \rightarrow \pi^*$ peak in the alloys containing higher Er and Cr contents do appear to be similar to those reported for the metal carbide phases such as chromium carbide and cementite.[11,12] Therefore, the increasing $1s \rightarrow \pi^*$ intensity with increasing Er and Cr additions in the $Fe_{65-x}Mo_{14}C_{15}B_6Er_x$ and $Fe_{65-x}Cr_xMo_{14}C_{15}B_6$ alloys is interpreted to result from the formation of carbidelike short-range order. Finally, it should be pointed out that there exists the possibility of formation of strong Er-B and Cr-B bonds. The latter could also participate in the local order described.

Considering the glass-forming ability, lanthanide elements, including Er, are reported to significantly enhance the glass-forming ability of Fe-based metallic glass by destabilizing the primary precipitated phase, $M_{23}(CB)_6$. This finding was attributed to the atomic strain effect due to the presence of large lanthanide atoms in $M_{23}(CB)_6$.[13] Previous work on a lanthanide effect through a series of chemical analyses showed that lanthanide elements partitioned away from $M_{23}(CB)_6$ particles during the early crystallization process.[14] The lanthanide effect on glass formability improvement can be further enhanced by the strong interatomic bonding that exists between Er and C atoms in the vitrified state. The strong Er-C bonding indicates that a higher energy and longer-range atomic redistribution is required to initiate precipitation of the $M_{23}(CB)_6$ phase, thus stabilizing the amorphous state and enhancing glass formability. In addition, as mentioned, the presence of Er-C local order could also improve the packing density in the vitrified state through the efficient packing of clusters, which contributes to the enhancement of the glass-forming ability.

C. Fe-$L_{2,3}$ edge results

The results of preferable Er-C and Cr-C bond formation can also be verified by investigating the Fe-$L_{2,3}$ edge spectra and Cr-$L_{2,3}$ edge spectra, respectively. Figure 4(a) shows the experimental EELS spectra of the Fe-$L_{2,3}$ edge corresponding to $Fe_{65-x}Mo_{14}C_{15}B_6Er_x$ amorphous alloys. All spectra are background subtracted and followed by plural scattering removal using the same conditions. General features are observed to be similar among all alloys with Er additions, including the edge position and shape. Further, EELS spectra of the Fe-$L_{2,3}$ edge exhibiting a similar shape and position are also observed for the $Fe_{65-x}Mo_{14}Cr_xC_{15}B_6$ amorphous alloys. (The results are not shown here.) For a quantitative comparison, the integrated white line intensities for L_2 and L_3 edges are calculated using the normalized method sug-

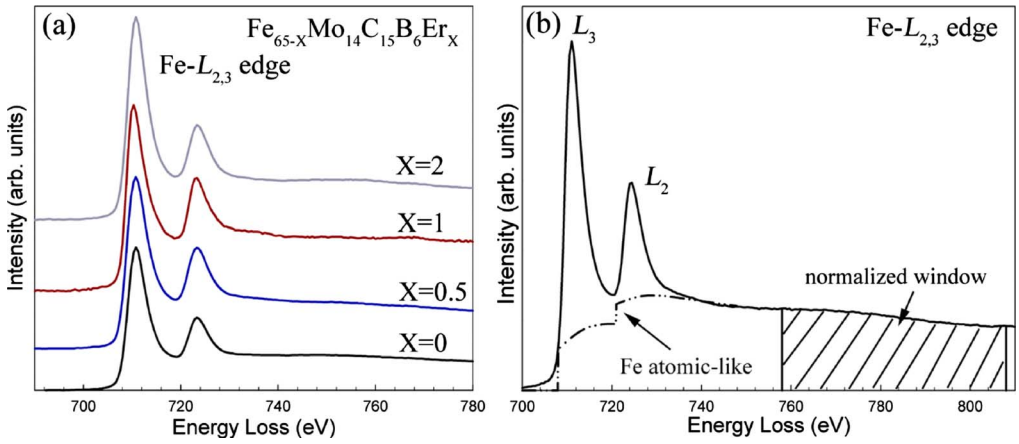

FIG. 4. (Color online) (a) The Fe-$L_{2,3}$ edge EELS spectra corresponding to $Fe_{65-x}Mo_{14}C_{15}B_6Er_x$ amorphous alloys, and (b) the Fe-$L_{2,3}$ edge superimposed with calculated Fe atomiclike cross sections and chosen normalized window.

gested by Pearson *et al.*[6] (In this paper, the energy ranges of 708–720 eV and 720–735 eV are selected for the L_3 and L_2 white line intensities calculations, respectively.) A normalized 50 eV window starting 50 eV beyond the L_3 threshold is used. All spectra are superimposed with the Fe atomiclike cross section calculated using the Hartree-Slater function. A representative spectrum illustrating the integrated white line intensities calculations is shown in Fig. 4(b). The calculated results, including the normalized area and the atomiclike cross section, are given in Table I. I_1 is the normalized cross section with atomiclike area and I_2 is the normalized cross section subtracted by the atomiclike section calculated by Rez.[15] All presented results are the averaged number obtained from more than ten spectra. Additionally, 3*d* electron occupancy of Fe in each alloy can be calculated by applying a linear correlation of the normalized white line intensity versus 3*d* occupancy determined by Pearson *et al.*[16] The equation is written as $I=1.06(1-0.094n)$, where I is the normalized white line intensity and n is the 3*d* occupancy, also referred to as electrons per atom. Applying this equation allows the calculation of n from the measured normalized white line intensity. The 3*d* electron occupancy results are also included in Table I.

TABLE I. Normalized cross sections and white line intensities of the Fe-$L_{2,3}$ edge for a series of Fe-based amorphous alloys. I_1 is the normalized cross section with atomiclike area and I_2 is the normalized cross section subtracted by the atomiclike section calculated by Rez. The calculated L_3/L_2 ratio and 3*d* occupancy are also listed.

Alloys	I_1	I_2	L_3/L_2 ratio	3*d* occupancy electrons/atom
$Fe_{65}Mo_{14}C_{15}B_6$	1.08	0.54	2.63	5.22
Atomiclike	0.54			
$Fe_{64.5}Mo_{14}C_{15}B_6Er_{0.5}$	1.04	0.52	2.74	5.42
Atomiclike	0.52			
$Fe_{64}Mo_{14}C_{15}B_6Er_1$	1.04	0.51	2.50	5.52
Atomiclike	0.53			
$Fe_{63}Mo_{14}C_{15}B_6Er_2$	1.05	0.51	2.52	5.52
Atomiclike	0.54			
$Fe_{59}Cr_6Mo_{14}C_{15}B_6$	1.10	0.55	2.36	5.12
Atomiclike	0.56			
$Fe_{50}Cr_{15}Mo_{14}C_{15}B_6$	1.11	0.54	2.33	5.22
Atomiclike	0.57			

From the results in Table I, the measured number of 3*d* electrons in Fe atoms increases slightly, that is, becomes more metallic, with increasing Er content. This can be explained as charge transfer occurring for metal-metalloid bonds as some outer 3*d* electrons of Fe atoms move towards C atoms. With the new introduction of Er atoms into the alloy, each Er atom, which has 11 4*f* electrons and a large negative heat of mixing with C and B, preferably forms strong bonds with C (B) and serves as an electron donor for C (B). This leads to the transferring of excess 4*f* electrons from Er to C (B), thereby reducing the electronegativity of C (B) atoms. As a result of redistribution of bonding electrons for carbon, some electrons are returned back to Fe atoms from C atoms, leading to the increase of 3*d* electrons in Fe. The observed increase in 3*d* electron occupancy of Fe with Er additions is consistent with the results of *ab initio* calculations performed by M. Widom *et al.*, who found an increase in the charge density around Fe atoms with Er additions.[17] The observation that Fe becomes more metallic with Er additions is also confirmed by x-ray photoemission spectroscopy (XPS), which shows peak splitting for the Fe 3*s* edge increasing towards that of metallic Fe with increasing Er additions.[18] In addition to the regain of charge by Fe atoms with Er additions, the other explanation for the increase of 3*d* electrons in Fe could be a result of the atomic size of Er. Specifically, preferable bonding between Er and C (B) atoms and the fairly large atomic size of Er might inhibit the formation of some Fe-C or Fe-B bonds and cause the reduction of the Fe-C (B) bond number. This is in good agreement with the results obtained by Inoue *et al.*,[4] who have reported that the coordination number of transition metals around an Fe atom in the Fe-based amorphous alloys decreases with the addition of lanthanide elements. Fewer coordination numbers of atoms means less bonding with metalloids and thus, fewer outer 3*d* electrons leaving Fe at-

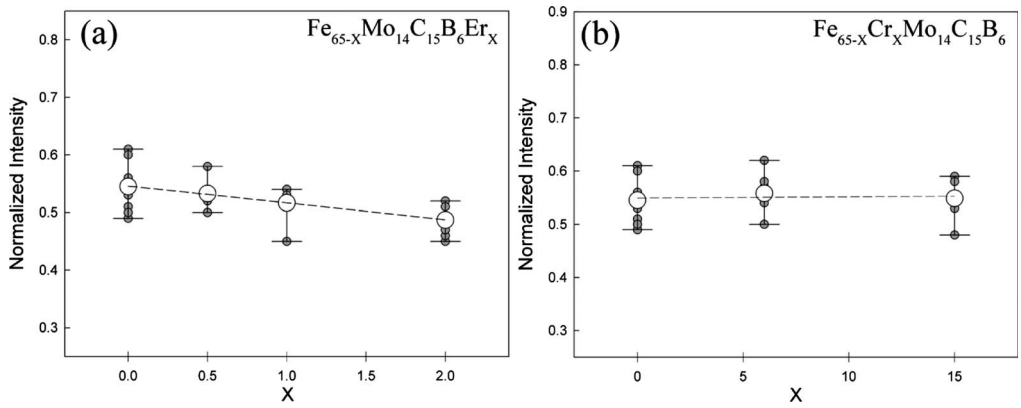

FIG. 5. Plots of Fe-3*d* integrated white line intensities as a function of (a) Er content for $Fe_{65-x}Mo_{14}C_{15}B_6Er_x$ amorphous alloys and (b) Cr content for $Fe_{65-x}Cr_xMo_{14}C_{15}B_6$ amorphous alloys.

oms, which coincides with the white line intensity calculation results of Fe with Er additions in the current Fe-Mo-C-B amorphous alloys.

As for Cr additions, not much difference is observed for the calculated 3*d* white line intensities of Fe when this element is added instead of Er. The calculated results for $Fe_{65-x}Cr_xMo_{14}C_{15}B_6$ amorphous alloys are also included in Table I, in which no noticeable charge transfer occurs around Fe atoms when Cr atoms are introduced into the alloys. This can be understood by noting that Cr has a similar atomic size with Fe, but fewer 3*d* electrons. Therefore, when Cr atoms are introduced into the alloys they simply replace some Fe atoms and form bonds with C (B) atoms because of their larger heat of mixing with metalloids as compared with Fe. However, Cr atoms do not serve as an effective electron donor as Er does and also has little effect on preventing Fe from forming bonds with C (B) because Cr and Fe have comparable atomic size. As a result, the 3*d* electron occupancy of Fe is not affected by the presence of Cr. This also suggests that the size effect of Ln is more plausible for the increase in Fe 3*d* occupancy upon adding Er. (According to the *ab initio* calculations of Fe-C compounds performed by Widom *et al.*,[17] the 3*d* electron charge densities around Fe atoms are expected to increase with Cr additions in the corresponding amorphous alloys. However, since a Cr atom is not as effective as an Er atom as an electron donor, any change in the electron densities around Fe atoms that might have occurred would be too small to be detected within the resolution of EELS measurement.) The 3*d* white line intensities plotted as a function of Er and Cr content are shown in Fig. 5. A clear trend of decreasing integrated 3*d* white line intensities, i.e., increasing 3*d* electron occupancy, with increasing Er content can be seen in Fig. 5(a), while no apparent variation in the integrated Fe 3*d* white line intensities for Cr additions is seen in Fig. 5(b).

In addition to the quantitative information on unoccupied 3*d* states, integrated white line intensity calculations can also offer some insight on the material's magnetic performance. Morrison *et al.*[19] reported a correlation that exists between magnetism and the L_3/L_2 ratio in amorphous Fe_xGe_{1-x} alloys, and found that the magnetic moment of Fe decreases with decreasing L_3/L_2 ratio.[20] As a result, the L_3/L_2 ratios calculated from Fe-$L_{2,3}$ edges in these amorphous alloys are also included in Table I in further verifying the white line intensity calculations. A slight reduction of L_3/L_2 ratio is observed for Er additions, while a larger decrease of the L_3/L_2 ratio is obtained for Cr introductions. This agrees with the magnetization measurement results performed in our group (unpublished). These results show that the Curie temperature decreases slightly when Er is added into the alloys, while a more significant reduction is obtained with Cr additions. The reductions of L_3/L_2 ratio and magnetic moment for both $Fe_{65-x}Mo_{14}C_{15}B_6Er_x$ and $Fe_{65-x}Cr_xMo_{14}C_{15}B_6$ amorphous alloys might be due to the interaction between Fe and Er and Fe and Cr atoms, respectively. Indeed, antiferromagnetic hyperfine interactions occurring between Fe 3*d* electrons and Er 4*f* electrons have been reported.[21,22] Also, 3*d*-3*d* electron interactions might occur between Fe and Cr, which cause the electron redistribution in Fe, resulting in the lowering of the magnetic moment significantly.

D. Cr-$L_{2,3}$ edge

The electronic structure of Cr is analyzed for both as-spun $Fe_{59}Cr_6Mo_{14}C_{15}B_6$ and $Fe_{50}Cr_{15}Mo_{14}C_{15}B_6$ amorphous alloys. The processed Cr-$L_{2,3}$ edges are shown in Fig. 6(a) for each alloy. A large difference in the Cr-$L_{2,3}$ edge intensity is observed between as-spun 6 and 15 at. % Cr amorphous alloys because of different Cr contents. The same method used to carry out the integrated white line intensity calculations for Fe is applied to Cr as well, except only a 10 eV window starting at 30 eV above the threshold energy of the L_3 edge is chosen for normalization as illustrated in Fig. 6(b). A 10 eV normalization window is used for the Cr edge so as to minimize the errors caused by low tailing background intensity because of low Cr contents. The calculated results are given in Table II. No difference is observed for the white line intensities and L_3/L_2 ratio between 6% and 15% Cr additions, indicating the same electronic environment around all Cr atoms in both alloys. This result reveals that all Cr atoms must have satisfied their bonding arrangement with C or B completely for both alloys regardless of the Cr content and thus leading to the same electronic structure around Cr for both alloys, indicating the occurrence of preferential bond formation between Cr and C.

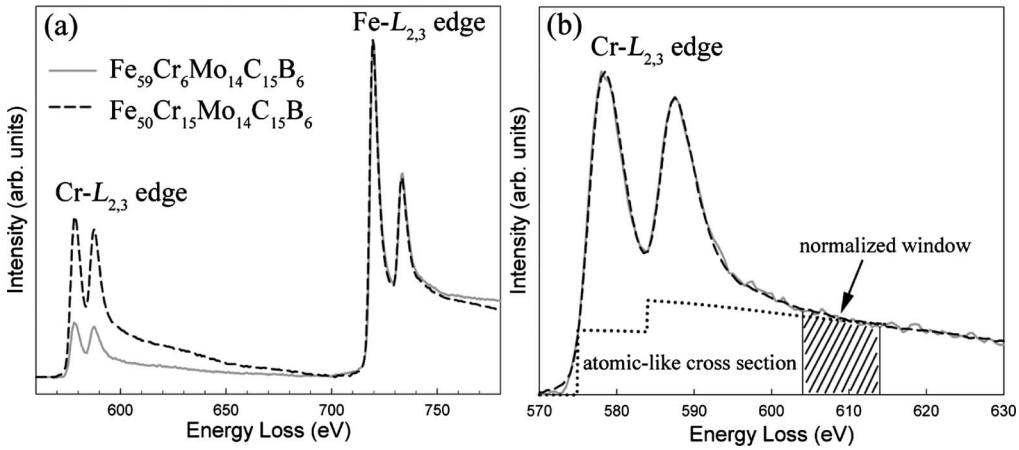

FIG. 6. (a) Cr-and Fe-$L_{2,3}$ EELS spectra of as-spun $Fe_{59}Cr_6Mo_{14}C_{15}B_6$ and $Fe_{50}Cr_{15}Mo_{14}C_{15}B_6$ amorphous alloys, and (b) redisplay of the Cr-$L_{2,3}$ edge with a larger energy scale superimposed with a calculated Cr atomiclike cross section and normalized window.

Low-loss EELS spectra for as-cast $Fe_{65-x}Mo_{14}C_{15}B_6Er_x$ and $Fe_{65-x}Cr_xMo_{14}C_{15}B_6$ amorphous alloys are presented in Fig. 7. A slight increase of plasmon peak energy is observed for both alloy systems when Er and Cr are added into the alloys. The results of measured plasmon peak energies are summarized in Table III along with reference data of pure Fe, Fe_2O_3, amorphous carbon, and graphite. From Table III, all of the amorphous alloys have the plasmon energy lying between amorphous carbon and graphite regardless of Er and Cr changes. The plasmon energy increases towards graphite with the additions of Cr and Er, which is very consistent with results concerning intensities of the $1s \rightarrow 1\pi^*$ transition peak as discussed in the C *K*-edge section. Therefore, the C *K* edge and plasmon energy are in good agreement with respect to increasing π bonding with Cr and Er additions.

E. Plastic-to-brittle transition discussion

It has been shown that amorphous metals that exhibit better ductility tend to have a lower shear modulus (G) to bulk modulus (K) ratio G/K.[1,2,23] Since $Fe_{65-x}Mo_{14}C_{15}B_6Er_x$ and $Fe_{65-x}Cr_xMo_{14}C_{15}B_6$ amorphous alloys show relatively large increases in G compared with much smaller changes in K at increasing x, the observed plastic-to-brittle trend associated with increasing Er and Cr contents can therefore be attributed to the increase in G.[1,2] That is, the increase in shear modulus is mainly responsible for the embrittlement of $Fe_{65-x}Mo_{14}C_{15}B_6Er_x$ and $Fe_{65-x}Cr_xMo_{14}C_{15}B_6$ amorphous alloys.

TABLE II. Normalized cross sections and white line intensities of the Cr-$L_{2,3}$ edge for a series of Fe-based amorphous alloys. I_1 is the normalized cross section with atomiclike area and I_2 is the normalized cross section subtracted by the atomiclike section calculated by Rez. The calculated L_3/L_2 ratio results are also listed.

Alloys	I_1	I_2	L_3/L_2 ratio
$Fe_{59}Cr_6Mo_{14}C_{15}B_6$	6.26	3.67	1.02
Atomiclike	2.59		
$Fe_{50}Cr_{15}Mo_{14}C_{15}B_6$	6.33	3.68	1.04
Atomiclike	2.65		

According to the solute-centered cluster model,[8] the carbon (and also boron) atoms occupy the interstitial sites of the atomic-cluster polyhedra and form bonds with their nearest neighboring Fe, Mo, Cr, and Er atoms. The clusters are connected to each other by sharing one or more metal atoms to form corner-, edge-, or face-sharing clusters, or by metal-metal bonds which form between the clusters. As a result, the types of short-range order in the present alloys are those of the intracluster metal-metalloid local order, as well as the Cr-C and Er-C local order mentioned above. Furthermore, it was found that the efficient packing of clusters could give rise to medium-range order in the amorphous structure.[9,10] Using the structural model described, the plastic-to-brittle transition occurring in $Fe_{65-x}Mo_{14}C_{15}B_6Er_x$ and $Fe_{65-x}Cr_xMo_{14}C_{15}B_6$ amorphous alloys can be explained by the formation of Cr-C and Er-C carbidelike local order. First, it is reasonable to assume that since the metal-metal bonds are appreciably weaker than the metal-metalloid bonds, the intercluster regions, where the weaker metal-metal bonds are located, are likely initiation sites for shear deformation. Upon adding Cr and Er to replace Fe, some of the weaker Fe-C (or Mo-C) carbide bonds in the corner-, edge-, or face-sharing clusters are replaced by stronger Cr-C and Er-C carbide bonds. With more and stronger, and presumably covalent, Cr-C and Er-C bonds, a growing number of solute-centered clusters become strongly connected. The strongly connected clusters impede shear deformation propagation and therefore tend to confine any applied shear stress to the more weakly bonded regions. As a result, the macroscopic shear modulus rises. The tendency for shear stress localization causes crack nucleation, resulting in brittle failure. Therefore, as the number of strongly connected clusters increase with increasing Er and Cr contents, the amorphous structure becomes progressively more brittle, as experiments verify.[1,2]

IV. CONCLUSIONS

Electronic energy-loss spectroscopy measurements were performed to investigate the electronic origin of the plastic-

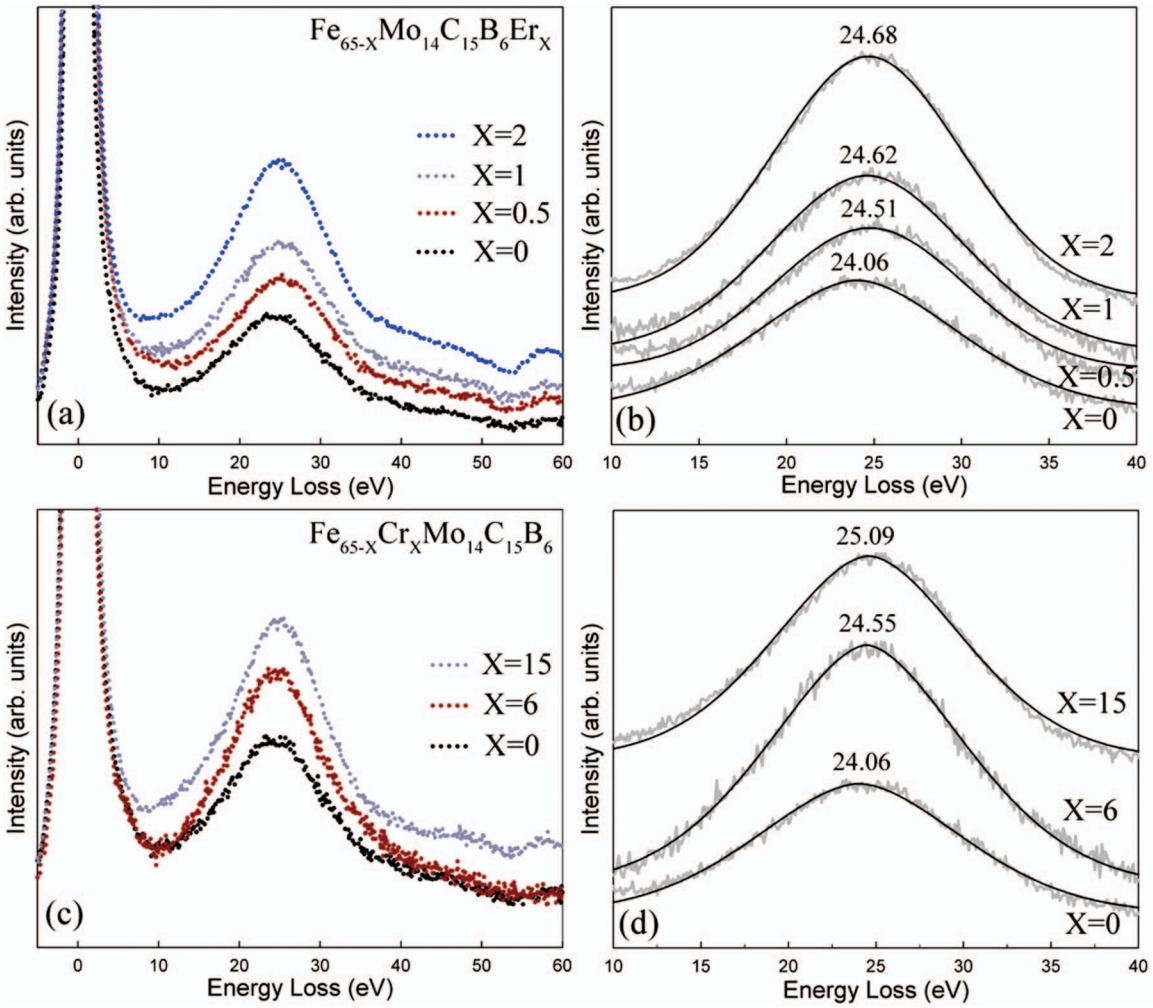

FIG. 7. (Color) (a) Zero-loss EELS spectra for $Fe_{65-x}Mo_{14}C_{15}B_6Er_x$ amorphous alloys, (b) the redisplay of the plasmon peak in expanded energy scale for (a), (c) zero-loss EELS spectra for $Fe_{65-x}Cr_xMo_{14}C_{15}B_6$ amorphous alloys, and (d) the redisplay of the plasmon peak in expanded energy scale for (c).

to-brittle transition in as-cast $Fe_{65}Mo_{14}C_{15}B_6$ amorphous alloys when Er or Cr solute is added to the alloy. The formation of an homogeneous amorphous phase in $Fe_{65-x}Mo_{14}C_{15}B_6Er_x$ and $Fe_{65-x}Cr_xMo_{14}C_{15}B_6$ amorphous alloys was verified by x-ray, electron diffraction, DSC, as well as high-resolution electron microscopy studies. A systematic EELS study revealed several key features of chemical bonding and charge transfer in these two amorphous alloy systems. Measurement of the C *K* edge showed the trend of increasing $1s \rightarrow \pi^*$ peak intensity with both Er and Cr additions. In view of the large heat of mixing between Er (Cr) and C atoms, the increase of π-bond character was ascribed to the preferential formation of Er-C and Cr-C bonds. The strong association between Er(Cr) and C atoms suggests that the Er and Cr atoms prefer to occupy the atomic sites shared by two or more metalloid-centered clusters in the amorphous structure, resulting in Er-C and Cr-C short-range order. At increasing Er and Cr contents, it was noted that the C *K*-edge spectra exhibiting a strong $1s \rightarrow \pi^*$ peak in alloys that contain higher Er and Cr contents do appear to be similar to those reported for chromium carbide and cementite.

TABLE III. Plasmon peak energy of $Fe_{65-x}Mo_{14}C_{15}B_6Er_x$ and $Fe_{65-x}Cr_xMo_{14}C_{15}B_6$ amorphous alloys. Reference data of pure Fe, Fe_2O_3, amorphous carbon, and graphite are also listed.

Alloys	Plasmon energy (eV)	Materials	Plasmon energy (eV)
$Fe_{65}Mo_{14}C_{15}B_6$	24.06	C (amorphous)	24
$Fe_{64.5}Mo_{14}C_{15}B_6Er_{0.5}$	24.51	C (graphite)	27
$Fe_{64}Mo_{14}C_{15}B_6Er_1$	24.62	Fe	23
$Fe_{63}Mo_{14}C_{15}B_6Er_2$	24.68	Fe_2O_3	21.8
$Fe_{59}Cr_6Mo_{14}C_{15}B_6$	24.55		
$Fe_{50}Cr_{15}Mo_{14}C_{15}B_6$	25.09		

The strong Er-C bond formation is responsible for the increase of 3*d* electron occupancy around Fe since Er atoms tend to donate electrons to C atoms, and therefore enables some electrons to be regained by Fe atoms. Additionally, the large size of the Er atoms also leads to the reduction of Fe-C bond population, which also contributes to the increase of 3*d* electrons in Fe. On the other hand, no noticeable charge transfer was observed with Cr additions. This is because Cr

atoms only possess four 3*d* electrons and do not serve as an effective electron donor as Er atoms do. Thus, the change of 3*d* white line intensities around Fe with Cr additions might be too small to be concluded from EELS.

The formation of strong Er-C or Cr-C covalent-like bonds in the amorphous structure provides an attractive explanation for the plastic-to-ductile transition found in Fe-based amorphous alloys. The metalloid-centered clusters are connected by strong Er-C and Cr-C bonds. The strongly connected clusters impede shear propagation. The tendency for shear stress localization leads to crack nucleation, resulting in brittle failure. Therefore, as the number of strongly connected clusters increase with increasing Er and Cr contents, the amorphous structure becomes more brittle. The present study demonstrates that the transition from plastic to brittle behavior in Fe-Mo-C-B amorphous alloys can be characterized through electronic structure analysis. It is also pointed out that effects from Mo and B atoms are neglected because of the difficulties in executing accurate EELS analysis on these two elements (relatively diluted B content and high Mo-$L_{2,3}$ edge energy) in Fe-Mo-C-B amorphous alloys. Consequently, further investigation of the electronic structure will require the incorporation of other techniques, such as x-ray photoemission spectroscopy (XPS), three-dimensional atom probe (3DAP), pair distribution function (PDF), and *ab initio* calculations. By combining these latter experimental and computational methods, results will lead to a more detailed understanding of the enbrittlement mechanism.

ACKNOWLEDGMENTS

The research is supported by the DARPA Structural Amorphous Metals Program under ONR Grant No. N00014-06-1-0492.

[1] X. J. Gu, A. G. McDermott, S. J. Poon, and G. J. Shiflet, Appl. Phys. Lett. **88**, 211905 (2006).
[2] X. J. Gu, S. J. Poon, and G. J. Shiflet, J. Mater. Res. **22**, 344 (2007).
[3] A. Inoue, A. Takeuchi, and B. L. Shen, Mater. Trans. **42**, 970 (2001).
[4] M. Imafuku, K. Yaoita, S. Sato, W. Zhang, and A. Inoue, Mater. Trans., JIM **40**, 1144 (1999).
[5] John Gilman, *Electronic Basis of the Strength of Materials* (Cambridge University Press, New York, 2003), p. 51.
[6] D. H. Pearson, B. Fultz, and C. C. Ahn, Appl. Phys. Lett. **53**, 1405 (1988).
[7] L. Ponsonnet, C. Donnet, K. Varlot, J. M. Martin, A. Grill, and V. Patel, Thin Solid Films **319**, 97 (1998).
[8] H. W. Sheng, W. K. Luo, F. M. Alamgir, J. M. Bai, and E. Ma, Nature (London) **439**, 419 (2006).
[9] A. P. Wang, J. Q. Wang, and E. Ma, Appl. Phys. Lett. **90**, 121912 (2007).
[10] D. B. Miracle, Nat. Mater. **3**, 697 (2004).
[11] K. He, A. Brown, R. Brydson, and D. V. Edmonds, J. Mater. Sci. **41**, 5235 (2006).
[12] S. Muto, T. Kimura, T. Tanabe, T. Kiyobayashi, and T. Maruyama, Jpn. J. Appl. Phys., Part 1 **44**, 2061 (2005).
[13] M. Mihalkovič and M. Widom, Phys. Rev. B **70**, 144107 (2004).
[14] H. J. Wang, Kenji Matsuda, Susumu Ikeno, S. J. Poon, and G. J. Shiflet, Appl. Phys. Lett. **91**, 141910 (2007).
[15] R. D. Leapman, P. Rez, and D. F. Mayers, J. Chem. Phys. **72**, 1232 (1980).
[16] D. H. Pearson, C. C. Ahn, and B. Fultz, Phys. Rev. B **47**, 8471 (1993).
[17] M. Widom (private communication).
[18] M. Büttner, H. J. Wang, A. M. Dongare, G. J. Shiflet, P. Reinke, P. Oelhafen, B. S. Mun, X. J. Gu, and S. J. Poon, J. Appl. Phys. **102**, 033501 (2007).
[19] T. I. Morrison, M. B. Brodsky, N. J. Zaluzec, and L. R. Sill, Phys. Rev. B **32**, 3107 (1985).
[20] D. M. Pease, A. Fasihuddin, M. Daniel, and J. I. Budnick, Ultramicroscopy **88**, 1 (2001).
[21] M. Ghafari and R. G. Escoto, Hyperfine Interact. **110**, 51 (1997).
[22] K. Szymanski, B. Kalska, D. Satula, L. Dobrzynski, A. Broddefalk, R. Wäppling, and P. Nordblad, J. Magn. Magn. Mater. **251**, 271 (2002).
[23] J. J. Lewandowski, W. H. Wang, and A. L. Greer, Philos. Mag. Lett. **85**, 77 (2005).